Fluorescent Polyimide Films Produced With Diatomite and Mesoporous Silica as Promising High-Tech Material

Riccardo Carlini (carlini@chimica.unige.it)
Artistic Academy https://orcid.org/0000-0001-5610-8967
Mohamed Ali Khalid
Yangzhou University
Yuxiang Yang
Yangzhou University
Yue Zhao
Yangzhou University
Xiangnong Liu
Yangzhou University
Eufrosina Garrone
LAS Klee-Barabino – Chemistry and Materials Chemistry
Anbang Dai
Nanjing University
Guangxiang Diao
Jilin Beinei Technology Co., Ltd

Research Article

Keywords: Films, Optical Properties, Self-Assembly, Synthesis and Processing Techniques

Posted Date: February 23rd, 2021

DOI: https://doi.org/10.21203/rs.3.rs-219172/v1

Abstract

Due to their excellent properties, polymides (PIs) result promising as high-performance materials in different technological fields. In this research, both micron-sized tubular mesoporous silica ($mSiO_2$) and double-tube tubular diatomite particles with cadmium sulfide quantum dots are prepared by chemical deposition method. A cluster of type fluorescent particles is prepared by self-assembling carbon quantum dots (CDs) on the inner surface of the above materials. Then, a fluorescent polyimide film is prepared by uniform dispersion of fluorescent particles.

The study of different properties of the film becomes then mandatory to evaluate possible application perspectives. Therefore, after synthesizes, all samples were investigated in term of chemical structure, microstructure and fluorescence properties by infrared spectroscopy, x-ray diffraction, scanning electron microscopy and fluorescence spectrophotometry.

Fluorescence performance of diatomite-based fluorescent particles (diatomite@CdS@CDs) results not as good as the $mSiO_2$-based fluorescent particles ($mSiO_2$@CdS@CDs) ones; the mechanical properties of the composite film deteriorate as the content of the inorganic component increases. The performance of PI/$mSiO_2$@CdS@CDs is 7.6 times the PI/diatomite@CdS@CDs ones.

Highlights

- Polymides show high-performance due to their outstanding thermal stability
- Mesoporous silica and diatomite represent ideal carriers for various nanoparticles
- Diatomite-based cluster fluorescent material can be used to prepare a composite fluorescent film first.

1. Introduction

Polymides (PIs) have been studied as high-performance materials due to their outstanding thermal stability, oxidative stress, chemical resistance, and excellent mechanical and electrical properties. They have been widely used in the field of gas separation, microelectronics, space devices, integrated electronic circuits, passivation coatings, substrate components, adhesives, composites and so on [1-2].

Composite materials studies have attracted increasing attention in the development of new functional materials for potential application fields which involve energy storage systems as super capacitors, sensing, catalysis, and drug delivery[3–6] for that, composites with nanostructured materials provide interactions between the different components, resulting in a material with combined properties which overcomes the disadvantages of the individual materials[7,8] ·Nowadays, combination between an organic, namely polymers, with an inorganic component, that is, metal nanoparticles or metal oxides, has offered novel nanocomposites with interesting properties in which a synergistic effect between the organic-inorganic components offer outstanding properties and performance[8] Examples of these

evidences have been observed in composite materials based on CdS, MnO_2, SnO_2, and IrO_2 with polymers, demonstrating remarkable performance in super capacitor applications, high sensitivity as gas-sensor, bioactive phases, and catalysis[9–11] .

Polyimide films showed significantly enhanced fluorescence emissions within the visible region owing to the suppression of the charge transition interactions through the introduction of alicyclic diamines.[12] However, these fluorescent Polyimides exhibit relatively small Stokes shifts, namely, an energy gap between the excitation (absorption) and emission wavelengths; consequently, a notable enhancement of the Stokes shifts is needed for photo luminescent polymers applied to solar-spectrum converters. We also reported that Polyimide films containing –OH exhibit a large Stokes-shifted fluorescence originating from the excited state through an intramolecular proton transfer [13-15].

Room-temperature phosphorescence in organic molecules has recently attracted significant attention owing to the resulting extremely large Stokes shifts and ultra-long luminescence lifetime [16,17]. Frequently, phosphorescence doesn't happen often at room temperature in air because it is easily deactivated by local molecular motion and energy transfer to oxygen during the ultra-long lifetime of the excited triplet state. There are two major strategies used to obtain room-temperature phosphorescence materials. One is to enhance the intersystem crossing efficiency by introducing heavy atoms such as metallic atoms and/or phenyl–carbonyl groups into the molecular structure. Such heavy atoms effectively enhance the intersystem crossing because of their large spin–orbit coupling, which is termed the “heavy-atom effect “[18]. Meanwhile, the incorporation of carbonyl groups facilitates intersystem crossing through the transitions allowed from 1 ($n \rightarrow \pi^*$) to 3 ($\pi \rightarrow \pi^*$) [19]. Another way is to reduce non-radioactive processes in an excited state by suppressing the local molecular motion, either by cooling to extremely low temperatures or by applying high pressure. For this reason, most room-temperature phosphorescence materials have been studied under cryogenic conditions below the temperature of liquid nitrogen in transparent rigid matrices such as crystalline compounds or in host–guest systems [20,21]. However, such systems are impractical for use in solar-spectrum converters.

Recently the field of flexible displays has seen a great development due to their applications in wearable devices, smartphones and other emerging displays. To obtain adequate efficiencies, however, it is necessary to know in depth the technical characteristics of these devices. That is the reason why this field is attracting the attention of many researchers whose aim is to develop new lines of basic research in order to solve the problems facing this industry. Interest in polymeric light-emitting materials is growing in this most crucial field due to their flexible nature and facile film formation by spin coating [22] or inkjet printing [23]. Conjugated polymers, such as poly(thiophene) [24] and polyfluorene [25] have become important light-emitting materials in large-area display devices, typically known as Polymer Light Emitting Diodes (PLEDs), BY showing great potential in advanced flexible displays.

CdS is a typical II-VI semiconductor compound with two crystal forms: a wurtzite type as a hexagonal phase and a sphalerite type as a cubic phase. It has a direct band gap of 2.42 eV, good response to

visible light, and good optical, photo physical and photochemical properties. Therefore, cadmium sulfide semiconductors can be considered promising materials in the fields of nonlinear optics and solar energy conversion, as photo catalysis, solar cells, etc. [26-30].

Fluorescent carbon quantum dots (CDs) are a new class of functional carbon nanomaterials and attracted great interest because of their versatile applications in optoelectronics, biomedical applications and chemical biosensors [31-33]. All Nano-sized fluorescent carbon materials with one dimension less than 10 nm can be classified as CDs, and these can be obtained from various carbon materials such as fullerenes, carbon nanotubes and graphene [34-36]. Conventional semiconductor quantum dots and organic dyes have the disadvantages of cumbersome preparation methods, high cost, toxicity and easy photo bleaching. Compared to them, CDs have high fluorescence efficiency, good water solubility, easy synthesis, low toxicity and, furthermore, good biocompatibility, high stability, surface modification capability and other advantages. They have a wide application value in many fields such as biology, chemistry and medicine [37-41]. Therefore, CDs have received more and more attention by the applied research at home and abroad so that various types of carbon quantum dots with excellent performance were developed: they are expected to become substitutes for traditional semiconductor quantum dots and organic dyes in the future.

Mesoporous silica material makes use of organic molecules (surfactants or amphiphilic block polymers) as a template: after the template is removed by calcinations or solvent extraction, the interface reacts with the inorganic silicon source to form a regular order system. The SiO_2 is assembled to form a porous nanostructure composite material retaining the inorganic skeleton of SiO_2. Due to its large specific surface area, high porosity, adjustable pore size, low material density, strong adsorption and assemblability, it shows broad application forecasts in the fields of catalytic carriers, gas adsorption and separation, drug delivery and chemical sensors [42].

It can be successfully developed thermally stable and highly transparent Room-temperature phosphorescence PIs with controlled optical properties, such as tunable luminescent colors, using a copolymerization technique. Such CoPIs are promising for light-emitting materials applicable to color tunable solid-state emitters, ratio metric oxygen sensors, and solar-spectrum converters [43] and also we have successfully fabricate highly thermally conductive and electrically insulating PI composite films filled with Graphene Oxide in three steps: in situ polymerization, self-assembly, and subsequent casting and thermal treatment [44].

A very interesting prospect could be to study a possible replacement material for SiO_2 that has better characteristics in terms of cost, manageability and eco-compatibility: diatomite seems to have these features. Diatomite is a material formed by the deposition of the remains skeletons of single-cell aquatic plants, the diatoms. Diatomite is a non-metallic mineral whose main chemical composition is amorphous silica, accompanied by a small amount of clay impurities such as Montmorillonite and Kaolinite, and organic matter. In Diatomite different shapes of algae can be seen under the microscope; each alga

varies in size from a few microns to several tens of microns, and they show many Nano-scale pores on their surface. Due to its porous structure, low density, large specific surface area, stable physic-chemical properties, strong adsorption performance, acid resistance, non-toxicity and odorless properties, diatomite has long been used as filters aid, thermal insulation material, anti-adhesive agent, desiccants. Furthermore, its abundance in mineral resources, wide source and low price make the China's diatomite a material widely used in various fields as carrier and functional filler.

Due to these excellent properties, mesoporous silica and diatomite have become ideal carriers for various nanoparticles. The combination of cadmium sulfide and silica matters not only has the advantages of low water absorption, low thermal expansion coefficient and high temperature resistance, but also has excellent fluorescent properties and enhances the performance of the composite film.

Therefore, in this research, mesoporous silica and diatomite are used as carriers to combine cadmium sulfide and carbon quantum dots on the surface, that are combined with polyimide, in a blending manner, to prepare a composite film with fluorescent properties. A characterization of different properties of the film is then carried out to evaluate possible application perspectives

2. Materials And Methods

2.1 Reagents

Pyromellitic dianhydride(PMDA) (purity ≥ 99.5%) by Jiangsu Hualun Chemical Co, Ltd4,4'-diaminodiphenyl ether(ODA) (purity ≥ 99.8%) by Dongying Guansen Insulation Products Co., Ltd.3-aminopropyltriethoxysilane(APS) (purity ≥ 98.0%) by Shanghai Dibo Chemical Reagent Co., Ltd. N,N-Dimethylacetamide(DMAc) (purity ≥ 99.0%), thiourea and absolute ethanol by Shanghai Titan Technology Co., Ltd. Citric acid(CA) (purity ≥ 99.0%), chromium chloride, sodium citrate(purity ≥ 99.0%), disodium edetate (EDTA) (purity ≥ 99.0%)by Shanghai Lingfeng Chemical Reagent Co., Ltd. Cetyltrimethylammonium bromide(CTAB) (purity ≥ 99.0%), tetraethyl orthosilicate(TEOS) (purity ≥ 98.0%) by Sinopharm Chemical Reagent Co., Ltd were used as reagents. The deionized water used for solutions was prepared in our laboratory.

2.2. Preparation of mesoporous silica

1.46 g of cetyltrimethylammonium bromide (CTAB) was weighed into a conical-flask and dissolved in 40 mL of deionized water, then 3.72 g of disodium edetate was added and mixed in magnetic stirrer. After stirring for 1 h, 4.5 mL of TEOS and 12 mL of absolute ethanol were poured into the above mixed system. After stirring for 30 minutes, the Erlenmeyer flask was transferred to a refrigerator and frozen at 5°C for 6 days to form a gel. After suction filtration, the product was washed three times with deionized water and dried in an oven at 60°C overnight. Finally, it was calcined at 550°C for 6 h in a muffle furnace to obtain white loose mesoporous silica.

2.3. Preparation of CdS

1 L 0.1 mol/L sodium citrate, $CdCl_2$ and thiourea solution were prepared for use, then 0.3 g of the mesoporous SiO_2 or diatomite prepared above were poured into a 500 mL three-necked flask, the prepared 20 mL sodium citrate solution was added, together with 250 mL of deionized water and 15 mL of $CdCl_2$ solution, to be mixed ultrasonically. An ammonia solution was added to reach a pH =11. Then, the solution was heated in a water bath and magnetically stirred at 60°C while a 30 mL thiourea solution was slowly added dropwise to the flask using a constant pressure dropping funnel and reacted for 2 hours. During the reaction, the color of the solution gradually changed from white to yellowish-green and then slowly changed to bright yellow. After the completion of the reaction, the mixture was centrifuged, the supernatant was removed, and the reaction product was washed three times with deionized water and ethanol, and finally dried under vacuum to obtain yellow $mSiO_2$@CdS and diatomite@CdS powder.

2.4. Preparation of CDs

0.3 g of prepared $mSiO_2$@CdS or diatomite@CdS, 0.04 g of citric acid, 0.80 mL of APS were added in a beaker, then 20 mL of deionized water was poured into the mixture to dissolve and homogenize the dispersion evenly the mixed suspension was transferred to a 50 mL stainless steel reaction kettle and placed in an oven at 180°C for 3 h. After the reaction was completed, the mixture was cooled to room temperature, and the product was centrifuged for 10 min in a high-speed centrifuge to remove the supernatant liquid, and the precipitate was repeatedly washed three times with ethanol and water to remove impurities, thereby obtaining $mSiO_2$@CdS@CDs and diatomite@CdS@CDs. The finally obtained $mSiO_2$@CdS@CDs and diatomite@CdS@CDs were dried in a vacuum drying oven, and the dried product was stored in the dark for use.

2.5. Preparation of fluorescent composite film

The 2.2248 g PMDA and 2.0024 g ODA were weighed separately using an analytical balance, and the molar ratio of PMDA to ODA was 1.02:1. First, 2.0024 g of ODA was poured into a 100 mL three-necked flask, and 36 mL of DMAc was weighed into a bottle and dissolved by mechanical stirring. The required amount of $mSiO_2$@CdS@CDs or diatomite@CdS@CDs was poured into a three-necked flask and stirred ultrasonically. After 30 minutes, 2.2248 g of PMDA was slowly poured into a three-neck bottle. As the amount of PMDA added increases, the viscosity of the system gradually increases. When the amount of PMDA added is close to that of ODA, the viscosity of the system increases sharply and the phenomenon of climbing is observed. After the addition of PMDA, mechanical stirring was continued for 6 hours to form a PAA hybrid solution. After the reaction, the solution was transferred to a jar for aging overnight, and then coated on a clean glass plate with a glass rod. The coated glass plate was placed in a vacuum drying box to evacuate and defoam, and then the glass plate was transferred to a high-temperature oven for thermal imidization to form a film. The specific heating process was carried out as follows: first heated at 60°C for 2 hours to remove the solvent, then heated at 80°C for 30 minutes, 130°C for 30 minutes, 180°C for 30 minutes, 250°C for 1 hour, 300°C was heated for 1 hour. Subsequently, the composite film was obtained by natural cooling to room temperature.

2.6. Experimental characterization

The Nicolet 6700 FT-IR infrared spectrometer from Nicol Corporation was used to measure the infrared spectrum of the composite film, with a scanning range of 4000-400 cm^{-1} and a resolution of 4 cm^{-1}. The XRD pattern of the film was measured by a R / D 2550 VB / PC X-ray diffract meter (Cu target Kα line, λ = 0.15406 nm) at room temperature. The diffraction line was filtered by a graphite monochromatic, and the tube pressure was 40 kV. The tube current is 35 mA. The scanning range is from 5° to 90°. The morphology of the fracture surface of the film was observed by Hitachi s4800 field emission scanning electron microscope (SEM), and the acceleration voltage was 15.0 kV. A Tecnai-12 (120 KV) transmission electron microscope (TEM) was used to observe the morphology of the samples. The fluorescence spectrum of the sample was measured using a FP-6500 fluorescence spectrometer manufactured by Japan Jasco Corporation. The film was cut into 6 cm × 1 cm strips. One end of the film was fixed with the ZQ-H24 tension fixture of Zhiqu Company, and the other end was put on a weight. The weight was increased until it broke, thus the breaking strength of the film was measured.

3. Results And Discussion

3.1 Infrared characterization

The infrared spectra of (a) mSiO_2@CdS@CDs and (b) diatomite@CdS@CDs are shown in Figure 1. Sample (a) shows absorption peak at 1061 cm^{-1} and sample (b) shows absorption at 1094 cm^{-1} correspond to the anti-symmetric stretching vibrations of Si-O-Si. The characteristic absorption peaks at 792 cm^{-1} in sample (a) and 793 cm^{-1} in sample (b) are generated from the symmetrical stretching vibration absorption of Si-O-Si, and the absorption peaks at 463 cm^{-1} in sample (a) and 476 cm^{-1} in sample (b) are due to the bending vibrations of Si-O-Si. The absorption peaks at 3421 cm^{-1} in sample (a) and 3446 cm^{-1} in sample (b) correspond to the stretching vibration absorption peaks of the N-H bond or the Si-OH bond one. The absorption peaks at 2935 cm^{-1} in sample (a) and 2924 cm^{-1} in sample (b) correspond to the C-H stretching vibration. On the other hand, the absorption peaks at 1630 cm^{-1} in sample (a) and 1633 cm^{-1} in sample (b) are characteristic absorption peaks of C=O, which are formed by the amide reaction of the amino group of APS with the carboxyl group of CDs, indicating that CDs were successfully coated on mSiO_2@CdS and On the surface of diatomite@CdS.

It can be seen from Figure 2 that the infrared spectra of (a) and (b) are approximately the same. The characteristic peaks of the imide group can be clearly seen from the Figure, where 1776 cm^{-1} in sample (a) and 1712 cm^{-1} in sample (b) are associated to C=O symmetrical and asymmetric stretching vibrations of the imide; at 721 cm^{-1} C=O bending vibration corresponds to imide and C-N symmetrical stretching vibration at 1366 cm^{-1}. This indicates that the polyimide has been completely formed. At the same time, a characteristic absorption peak of Si-O-Si appears at 1087 cm^{-1}, and a bending vibration peak of Si-OH appears at 936 cm^{-1}: this indicates that the compound contains SiO_2.

3.2 XRD characterization

Observing Figure 3, obvious diffraction peaks appear at 2θ = 26.6°, 31.2°, 44.3°, and 51.9°. By comparison with the standard XRD spectrum (JCPDS card number 80-0019), can be observed that these peaks correspond to the (111), (200), (220), (311) crystal planes of the CdS of the cubic sphalerite structure: this shows that the product contains CdS. In addition, diatomite@CdS@CDs has a stronger CdS characteristic diffraction peak than $mSiO_2$@CdS@CDs, indicating that the crystallinity of CdS is better on diatomite than on $mSiO_2$.

It can be observed from the spectrum reported in Figure 4 that PI has a broad peak between 12°-27°, without obvious sharp diffraction peaks, and a diffused peak with a gimmick-like shape, indicating that the PI is less ordered and less crystalline than the other compounds. Compared with pure polyimide films, the synthesized doped $mSiO_2$@CdS@CDs and diatomite@CdS@CDs composite films are also similar to the pure PI peak shape, but the crystalline peak height is reduced. The introduction of $mSiO_2$@CdS@CDs and diatomite@CdS@CDs hybridization factors into the PI matrix destroys the molecular regularity of PI preventing the inorganic phase from existing in a crystalline state. These results indicate that, in the obtained product, the crystallinity of $mSiO_2$@CdS@CDs and diatomite@CdS@CDs is not very good. The inorganic phase is dispersed in the polyimide matrix with an amorphous structure, thereby further increasing the disorder of the film.

3.3.TEM characterization

Dense black spots distributed on the surface of mesoporous silica can be well observed in Figure 5a. Furthermore, it can be seen from Figure 5b that the particle size of the cadmium sulfide nanoparticles is about 30-40 nm. Figures 5c and 5d report TEM images of $mSiO_2$@CdS@CDs formed after carbon quantum dots are loaded on the surface of $mSiO_2$@CdS. It can be seen from Figure 5c that the distribution of cadmium sulfide and carbon dots in the mesoporous silica is relatively uniform. In addition to the large CdS nanoparticles shown in Figure 5d, smaller black spots can also be seen: this should justify that the carbon quantum dot has been successfully loaded. From Figures 5e and 5f it can be clearly observed that the spherical cadmium sulfide nanoparticles are on the surface of the diatomite, and the particles size of the cadmium sulfide nanoparticles is about 40 nm. Figure 5h shows some small black spots on the surface in addition to cadmium sulfide: this indicates the carbon points have been successfully loaded on the surface of diatomite.

3.4. SEM characterization

The obtained mesoporous silicas all appear as tubular structures of varying lengths and thicknesses, as showed in Figure 6a. Comparing Figure 6a and 6b, the surface of mesoporous silica in Figure 6b has obvious “protrusions”, which appear a little rough, justified by the deposition of the CdS compound on the surface of mesoporous silica. Magnification, can be clearly seen from Figure 6d where the surface of

mesoporous silica is covered with uniformly distributed and sized CdS particles, having a particle size of about 30-40 nm: this results in in full agreement with the result obtained from the TEM characterization.

As can be seen from Figures 7a and 7b, CdS nanoparticles are intricately distributed throughout the mesoporous silica and are disorderly embedded in the PI matrix: a phase separation can be also clearly seen. The images observed in Figures 7c and 7d are similar the ones reported in Figures 7a and 7b. Diatomite and PI are cross-linked and CdS nanoparticles are randomly distributed in them. The size of CdS nanoparticles is the same as the ones above observed, and their size is between 30 and 40 nm. These results show that the dispersibility of the inorganic phase in PI/mSiO_2@CdS@CDs and PI/diatomite@CdS@CDs, prepared by mechanical blending,

3.5. Fluorescence spectrum characterization

The maximum emission wavelengths, corresponding to the studied compounds, are well shown Figure 8. It can be seen that under the same conditions, the maximum emission wavelength of mSiO_2@CdS is about 542 nm and the fluorescence emission intensity is about 1.410^6×. After loading the carbon quantum dots, the maximum emission wavelength of mSiO_2@CdS@CDs is seen to be 540. The values differ only by a few nm, the fluorescence peak intensity increased to 2.710^6× while the intensity increased by 1.78 times. If compared with mSiO_2@CdS, the maximum emission wavelength of diatomite@CdS is 548 nm: this result is also substantially unchanged. The fluorescence emission intensity is only 0.610^5×, and the fluorescence intensity drops to 22%. This may be due to the quenching of fluorescence by diatomite containing metal ions such as iron. After the diatomite@CdS was loaded with CDs, the maximum emission wavelength of the generated diatomite@CdS@CDs hardly changes, while the fluorescence intensity increases to 5.010^5× and the intensity increases by 1.78 times, the same one of mesoporous silica.

15% mSiO_2@CdS@CDs and diatomite@CdS@CDs PI composite film and pure PI film were tested for fluorescence. The corresponding maximum emission wavelength is shown in Figure 9. It can be seen that the obtained film has good light emitting properties. Furthermore, under the same conditions, the maximum emission wavelength of pure PI film is about 468 nm, and the emission peak intensity is only about 35890 counts. The maximum emission wavelength of the PI/mSiO_2@CdS@CDs composite film is 546 nm and the fluorescence emission intensity is about 920900 counts, while the maximum emission wavelength of the PI/diatomite@CdS@CDs composite film is 545 nm and the fluorescence emission intensity is 120470. If compared with PI/mSiO_2@CdS@CDs composite film, the gap is larger, but the fluorescence intensity is still larger than the pure PI one. This indicates that the good luminescence property here observed should mainly come from SiO_2@CdS@CDs and diatomite@CdS@CDs: they act as a luminous center in them. On the other hand, the performance of PI/mSiO_2@CdS@CDs is 7.6 times that of PI/diatomite@CdS@CDs, which is mainly due to the presence of iron in diatomite.

Table 1 X-ray fluorescence spectral data results of diatomite

Compounds	SiO_2	Al_2O_3	Fe_2O_3	Na_2O	K_2O	CaO
Content	92.0303%	2.5947%	2.4385%	1.9032%	0.5725%	0.4608%

3.6. TG characterization

From the curve reported in Figure 10 it can be seen that 5% of pure PI film thermal loss leads to a temperature of 534°C. The curve b corresponds to the thermogravimetric curve of the composite film after adding 10% mSiO_2@CdS@CDs. The curve does not change too much. 5% thermal loss of PI/mSiO_2@CdS@CDs composite film leads to a temperature of 547°C: the decomposition temperature slightly increases. After adding 10% of diatomite@CdS@CDs, it can be found from the curve c that the heat resistance of the composite film has greatly decreased. When 5% heat loss of the PI/diatomite@CdS@CDs film is reached a temperature of 430°C can be measured. This may be because the diatomite in the PI/diatomite@CdS@CDs composite film contains large particles of impurities that are unevenly dispersed in the PI: this behavior promotes a destruction of the molecular chain structure of the PI and reduces the heat resistance of the composite film.

3.7. Mechanical behavior characterization

The breaking strength test shows that the breaking strength of the composite film has a downward trend when the content of mSiO_2@CdS@CDs and diatomite@CdS@CDs increases: it can be observed in Figure 11. At the same content level, PI/diatomite@CdS@CDs film has lower mechanical strength than PI/mSiO_2@CdS@CDs film. When the content of the added inorganic component is 5%, the breaking strength of the composite film is not very different from the pure PI one, even if it is slightly reduced. When the content gradually increases, the breaking strength of the composite film decreases rapidly. This trend is because the inorganic phase in the composite film easily aggregates, which destroys the molecular chain structure of the polyimide, thereby reducing the intermolecular force of polyimide as previously described.

The reason why the mechanical strength of the PI/diatomite@CdS@CDs film is worse than the PI/mSiO_2@CdS@CDs one may be because the large particles of impurities in the diatomite further damage the polyimide molecular chain and make the film strength worse.

4. Conclusion

Mesoporous silica and diatomite are been used as carriers to combine cadmium sulfide and carbon quantum dots on the surface, combined in turn with polyimide to prepare a composite fluorescent film. The results show that the prepared CdS quantum dots and carbon quantum dots are uniformly dispersed in mSiO_2 and diatomite. The size of CdS nanoparticles is about 30-40 nm, and they have excellent fluorescence performance. In contrast, the fluorescence performance of diatomite-based fluorescent

particles (diatomite@CdS@CDs) is not as good as the $mSiO_2$-based fluorescent particles ($mSiO_2$@CdS@CDs) ones. When they are incorporated into polyimide films, their fluorescence performance decreases, in fact, the fluorescence performance of PI/$mSiO_2$@CdS@CDs is not as good as $mSiO_2$@CdS@CDs. Furthermore, the mechanical properties of the obtained composite film deteriorate as the content of the inorganic component increases. In spite of the results, this research shed light on the behavior of diatomite as a precursor of other promising composite materials. This encourages further investigation of these materials by introducing changes in the size of the carbon quantum dots or replacing the CdS with more performing compounds.

Declarations

Acknowledgments

The authors are grateful to the National Natural Science Foundation of China for their financial support (Grant No. 29201004).

References

1. K. Faghihi, A. Feyzi, H.N. Isfahani, Design. Monom. Polym. **13**, 131–142 (2010)
2. H.Y. Huang, T.C. Huang, T.C. Yeh, C.Y. Tsai, C.L. Lai, M.H. Tsai, J.M. Yeh, Y.C. Chou, Polym. **52**, 2391–2400 (2011)
3. S. Thanjam, M.F. Philips, S. Komathi, P. Manisankar, C. Sivakumar, A. Gopalan, K.-P. Lee, Spectrochim. Acta Part A Mol. Biomol. Spectrosc. **79**, 1256 (2011)
4. M.El Rhazi, S. Majid, M. Elbasri, F.E. Salih, L. Oularbi, K. Lafdi, Int. Nano Lett. **8**, 79 (2018)
5. R. Ojani, J.B. Raoof, Y.A. Khanghah, S. Safshekan, Int. J. Hydrogen Energy **38**, 5457 (2013)
6. R. Ojani, J.B. Raoof, Y.A. Khanghah, Electrochim. Acta **56**, 3380 (2011)
7. H. Xu, J. Tang, Y. Chen, J. Liu, J. Pu, Q. Li, J. Electron. Mater. **46**, 6150 (2017)
8. S. Sarkar, E. Guibal, F. Quignard, A.K. SenGupta, J. Nanopart. Res. **14**, 715 (2012)
9. W. Gao, Z. Li, 21-Nanostructured transition metal oxides and their applications in composites, in *Woodhead Publishing Series in Composites Science and Engineering*, ed. by S.C. Tjong, Y.-W. Mai (Woodhead Publishing, New Zealand, 2010), p. 723
10. K. Subhash Baburao, S.P. Agrawal, S.H. Nimkar, H.J. Sharma, P.T. Patil, Adv. Mater. Lett. **3**(5), 396 (2012)
11. J. Moral-Vico, S. Sánchez-Redondo, M.P. Lichtenstein, C. Suñol, N. Casañ-Pastor, Acta Biomater. 10(2014) 2177
12. J. Wakita, H. Sekino, K. Sakai, Y. Urano, S. Ando, Molecular Design, Synthesis, and Properties of Highly Fluorescent Polyimides. J. Phys. Chem. B **113**, 15212–15224 (2009)

13. J. Wakita, S. Inoue, N. Kawanishi, S. Ando, Excited-State Intramolecular Proton Transfer in Imide Compounds and Its Application to Control the Emission Colors of Highly Fluorescent Polyimides. Macromolecules **43**, 3594–3605 (2010)
14. K. Kanosue, T. Shimosaka, J. Wakita, S. Ando, Polyimide and Imide Compound Exhibiting Bright Red Fluorescence with Very Large Stokes Shifts via Excited-State Intramolecular Proton Transfer. Macromolecules **48**, 1777–1785 (2015)
15. K. Kanosue, R. Augulis, D. Peckus, R. Karpicz, T. Tamulevicius, S. Tamulevicius, V. Gulbinas, S. Ando, Polyimide and Imide Compound Exhibiting Bright Red Fluorescence with Very Large Stokes Shifts via Excited-State Intramolecular Proton Transfer II. Ultrafast Proton Transfer Dynamics in the Excited State. Macromolecules **49**, 1848–1857 (2016)
16. S. Hirata, Recent Advances in Materials with Room Temperature Phosphorescence: Photophysics for Triplet Exciton Stabilization. Adv. Opt. Mater **5**, No. 1700116 (2017)
17. L. Xiao, Z. Chen, B. Qu, J. Luo, S. Kong, Q. Gong, Recent Progresses on Materials for Electrophosphorescent Organic LightEmitting Devices. Adv. Mater. **23**, 926–952 (2011)
18. H. Shi, Z. An, P.Z. Li, J. Yin, G. Xing, T. He, H. Chen, J. Wang, H. Sun, W. Huang, Y. Zhao, Enhancing Organic Phosphorescence by Manipulating Heavy-Atom Interaction. Cryst. Growth Des. **16**, 808–813 (2016)
19. S. Kuno, H. Akeno, H. Ohtani, H. Yuasa, Visible RoomTemperature Phosphorescence of Pure Organic Crystals via a Radicallon-Pair Mechanism. Phys. Chem. Chem. Phys. **17**, 15989–15995 (2015)
20. R. Gahlaut, H.C. Joshi, N.K. Joshi, N. Pandey, P. Arora, R. Rautela, K. Suyal, S. Pant, Luminescence Characteristics and Room Temperature Phosphorescence of Naphthoic Acids in Polymers. J. Lumin. **138**, 122–128 (2013)
21. D. Lee, O. Bolton, B.C. Kim, J.H. Youk, S. Takayama, J. Kim, Room Temperature Phosphorescence of Metal-Free Organic Materials in Amorphous Polymer Matrices. J. Am. Chem. Soc. **135**, 6325–6329 (2013)
22. S.A. Haque, S. Koops, N. Tokmoldin, J.R. Durrant, J. Huang, D.D.C. Bradley, E. Palomares, Advanc. Mater. **19**(5), 683–687 (2007)
23. R. Satoh, S. Naka, M. Shibata, H. Okada, H. Onnagawa, T. Miyabayashi, T. Inoue, Jpn. J. Appl. Phys. **43**(11A), 7725–7728 (2004)
24. I.F. Perepichka, D.F. Perepichka, H. Meng, F. Wudl, Advanc. Mater. **17**(19), 2281 (2005)
25. J. Liu, J. Zou, W. Yang, H. Wu, C. Li, B. Zhang, J. Peng, Y. Cao, Chem. Mater. **20**(13), *4499*–4506 (2008)
26. A.E. Raevskaya, O.L. Stroyuk, D.I. Solonenko et al., J. Nanopart. Res. **16**(10), 2650 (2014)
27. E.A. Raevskaya, O.L. Stroyuk, Y.V. Panasiuk et al., Nano-Obj. **85**(2), 26–28 (2015)
28. A. Aboulaich, D. Billaud, M. Abyan et al., Acs Appl. Mater. Interf. **4**(5), 2561 (2012)
29. T.D. Nguyen, W.Y. Hamad, M.J. Maclachlan, Adv. Funct. Mater. **24**(6), 777–783 (2014)
30. H. Li, L. Guan, T. Liu et al., Ind. Eng. Chem. Res. **46**(7), 2013–2019 (2007)

31. J.C.E. Da Silva, H.M. Gonçalves, Anal. Chem. **30**, 1327–1336 (2011)
32. X.T. Zheng, A. Ananthanarayanan, K.Q. Luo, P. Chen, Small **11**, 1620–1636 (2015)
33. Y. Dong, J. Cai, X. You, Y. Chi, Analyst **140**, 7468–7486 (2015)
34. S. Zhu, Y. Song, X. Zhao, J. Shao, J. Zhang, B. Yang, Nano Res. **8**, 355–381 (2017)
35. P. Namdari, B. Negahdari, A. Eatemadi, Biomed. Pharmacot. **87**, 209–222 (2017)
36. H. Tao, K. Yang, Z. Ma, J. Wan, Y. Zhang, Z. Kang, Z. Liu, Small **8 2**, 81–290 (2012)
37. H. Liu, Z. He, L.P. Jiang et al., Appl. Mater. Interf. **7**(8), 4913–4920 (2015)
38. S. Mondal, P. Purkayastha, J. Phys. Chem. C **120**(26), 14365–14371 (2016)
39. F. Wang, S. Pang, L. Wang et al., Chem. Mater. **22**(16), 4528–4530 (2010)
40. A.B. Bourlinos, R. Zboril, J. Petr et al., Chem. Mater. **24**(1), 6–8 (2011)
41. C.W. Lai, Y.H. Hsiao, Y.K. Peng et al., J. Mater. Chem. **22**(29), 14403–14409 (2012)
42. H. Song, H.L. Feng, X.L. Sun, Chin. Ind. Catal. **18**(9), 1–6 (2010)
43. M. Nara, R. Orita, R. Ishige, S. Ando, ACS Omega **5**, 14831–14841 (2020)
44. X. He, Y. Wang, Ind. Eng. Chem. Res. **59**, 1925–1933 (2020)

Figures

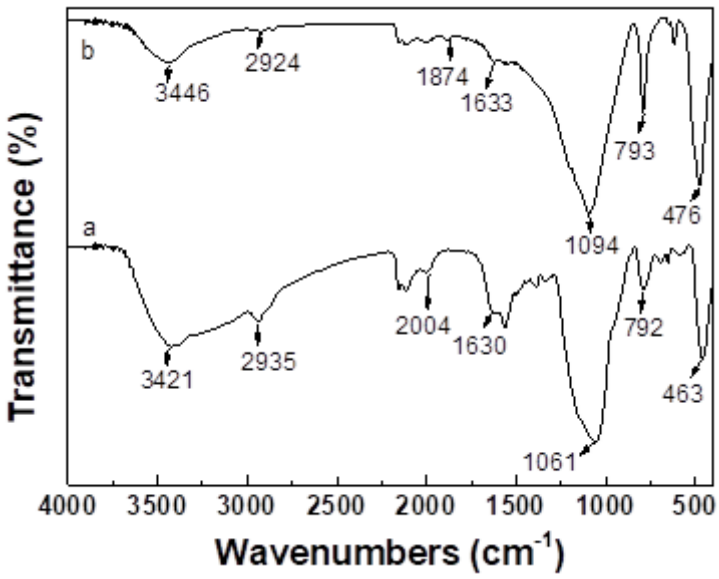

Figure 1

FT-IR spectra of (a) mSiO2@CdS@CDs, (b) diatomite@CdS@CDs

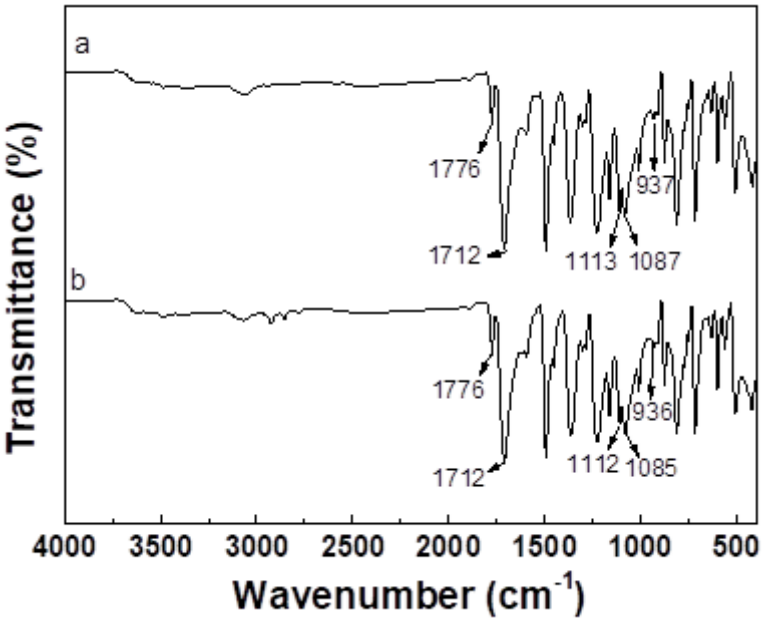

Figure 2

FT-IR spectra of (a) PI/mSiO2@CdS@CDs and (b) PI/diatomite@CdS@CDs

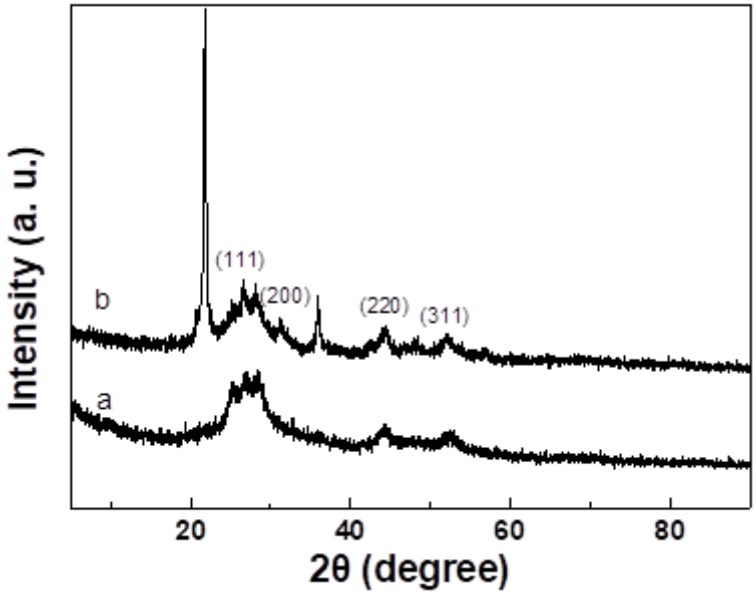

Figure 3

XRD pattern of (a) mSiO2@CdS@CDs, (b) diatomite@CdS@CDs

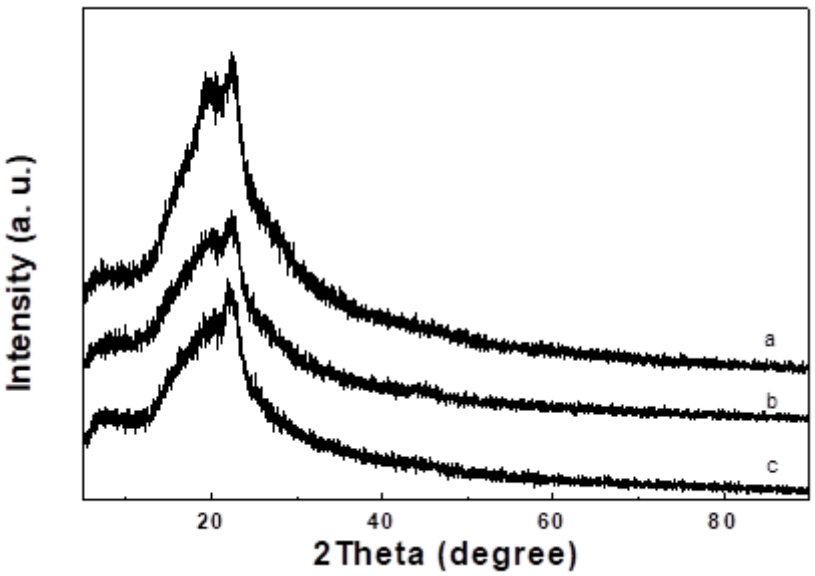

Figure 4

XRD pattern of (a) pure PI, (b) PI/mSiO2@CdS@CDs, (c) PI/diatomite@CdS@CDs

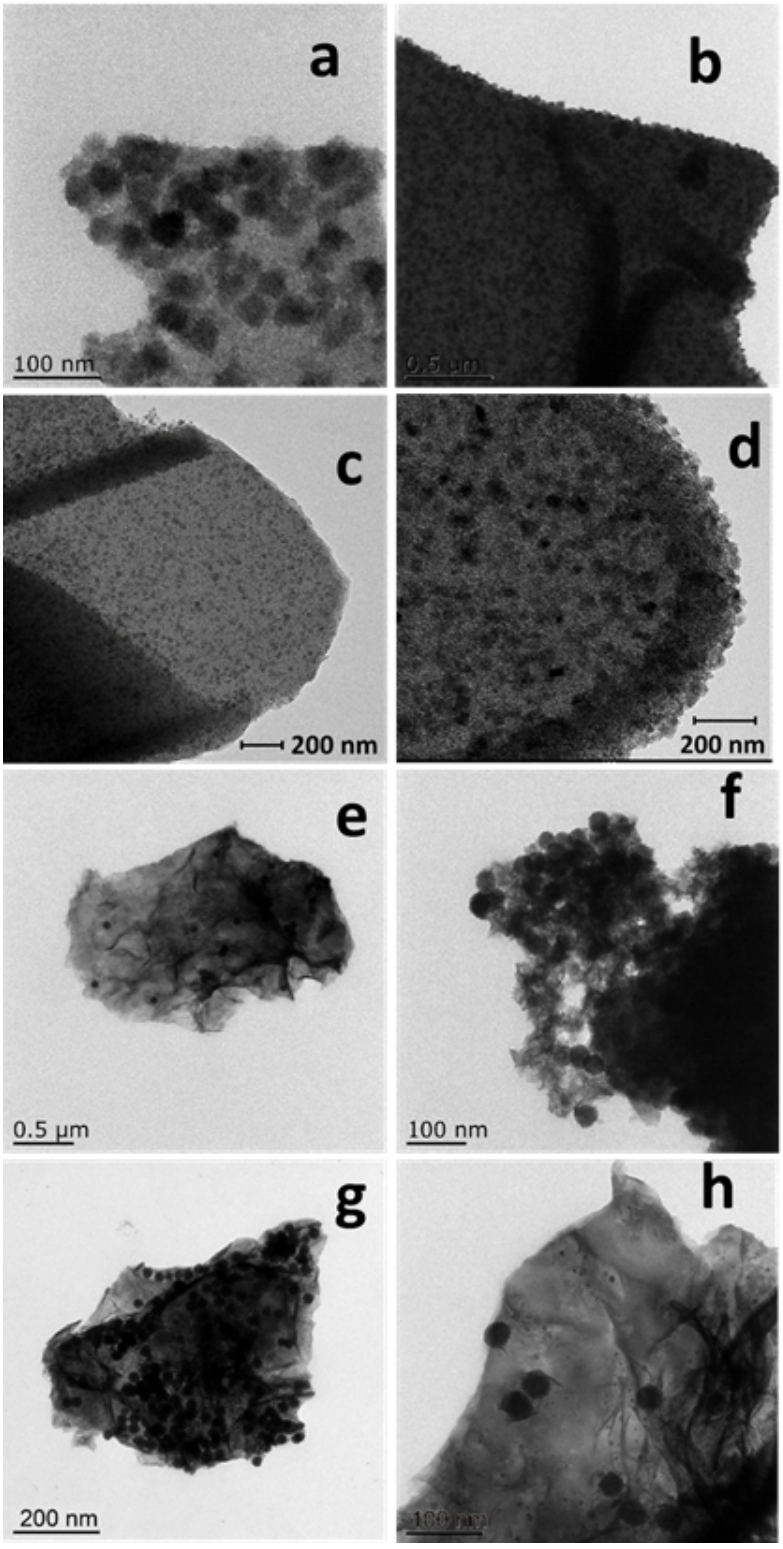

Figure 5

TEM images of (a) and (b) mSiO2@CdS, (c) and (d) mSiO2@CdS@CDs, (e) and (f) diatomite@CdS, (g) and (h) diatomite@CdS@CDs

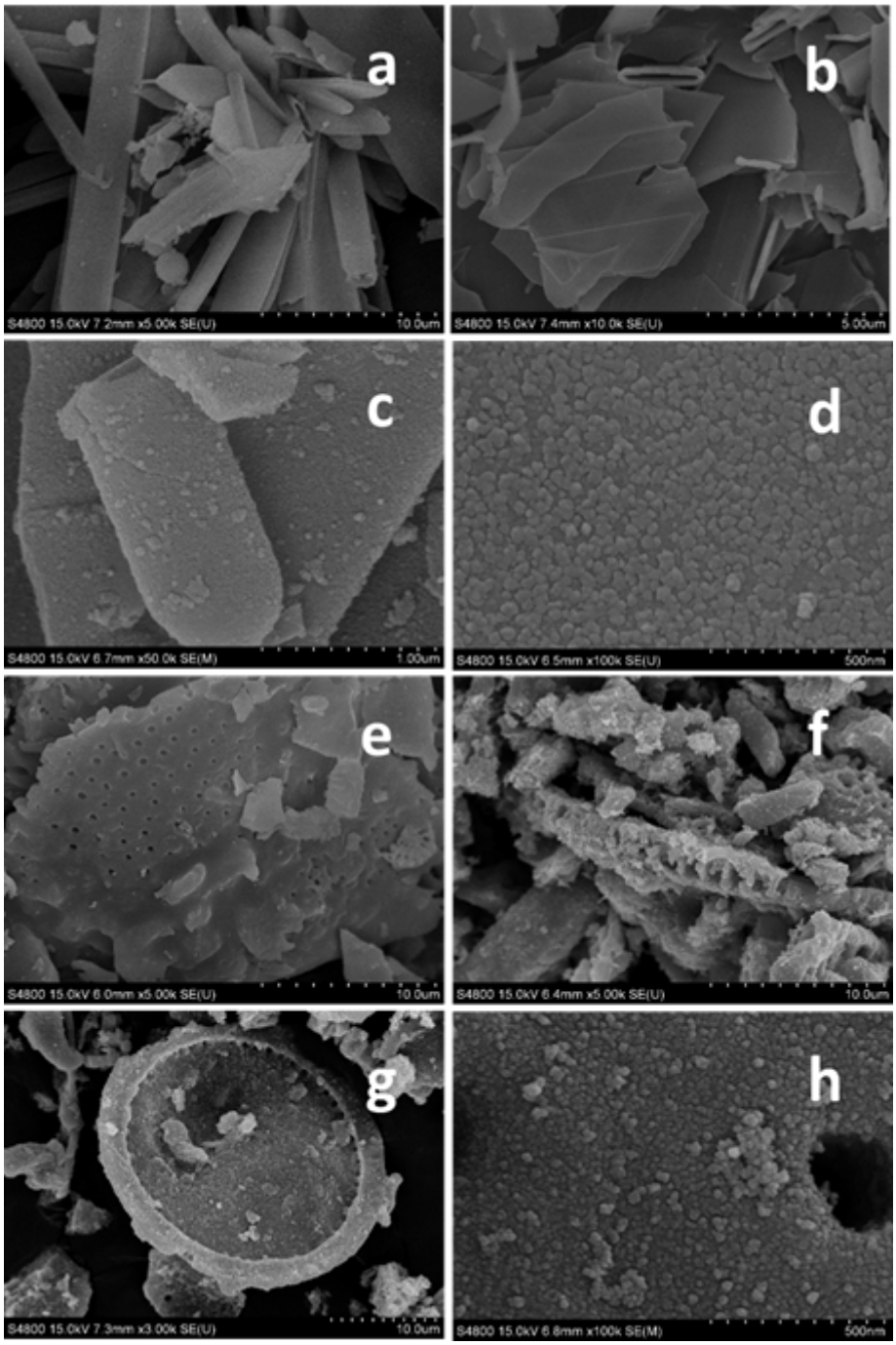

Figure 6

SEM images of (a) mSiO2, (b) mSiO2@CdS, (c) and (d) mSiO2@CdS@CDs, (e) diatomite, (f) diatomite@CdS, (g) and (h) diatomite@CdS@CDs

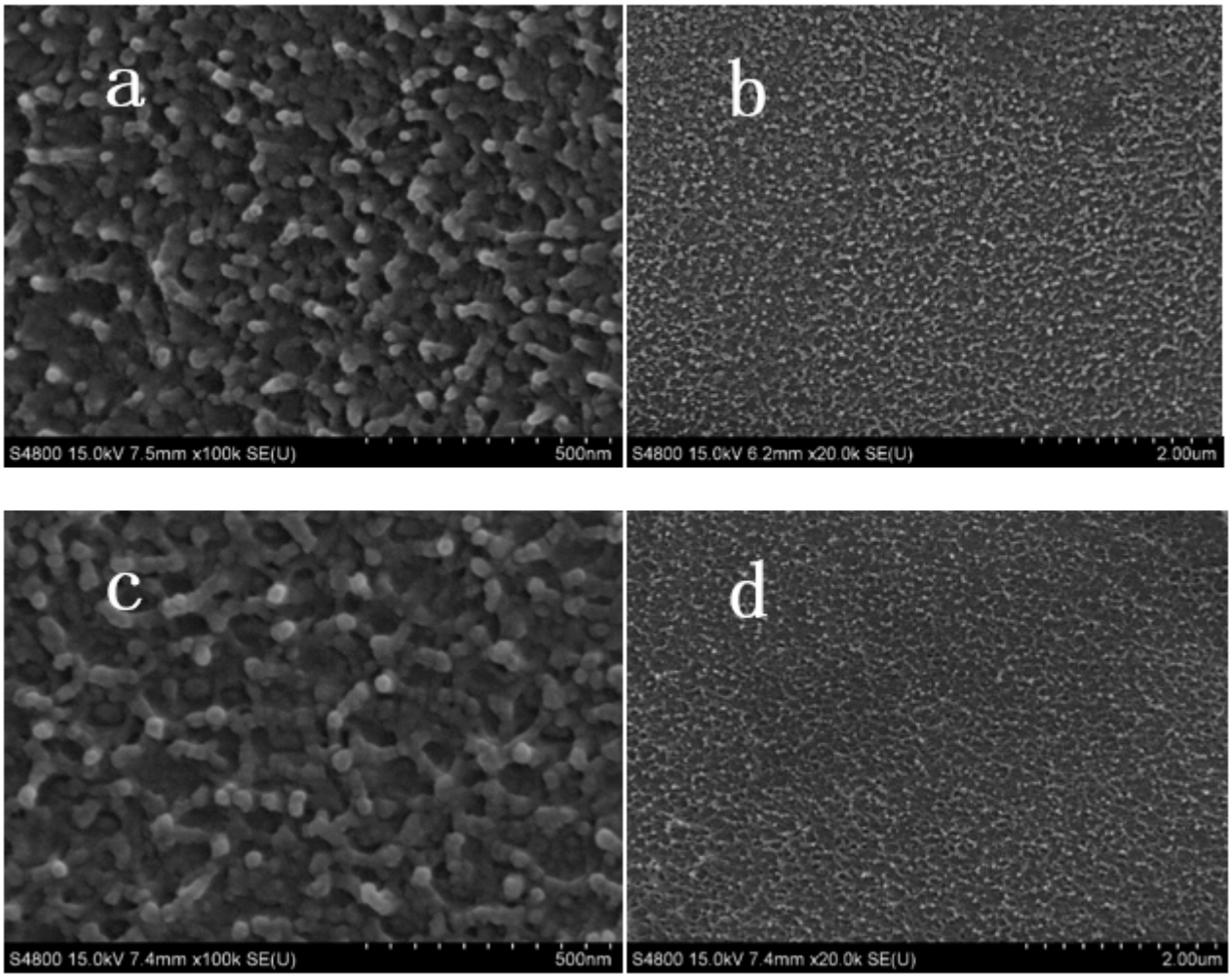

Figure 7

SEM images of PI/mSiO2@CdS@CDs in (a) and (b), PI/diatomite@CdS@CDs in (c) and (d)

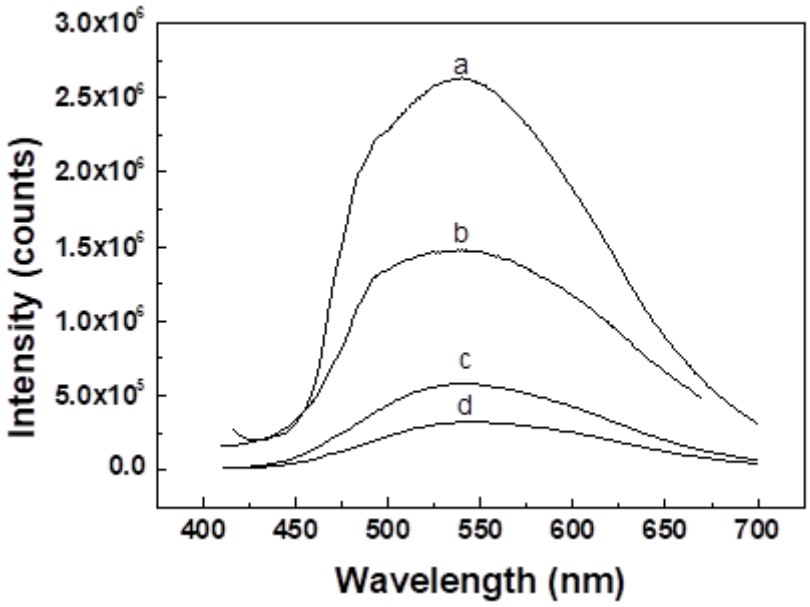

Figure 8

Fluorescence emission spectrum of (a) mSiO2@CdS@CDs, (b) mSiO2@CdS, (c) diatomite@CdS@CDs, (d) diatomite@CdS

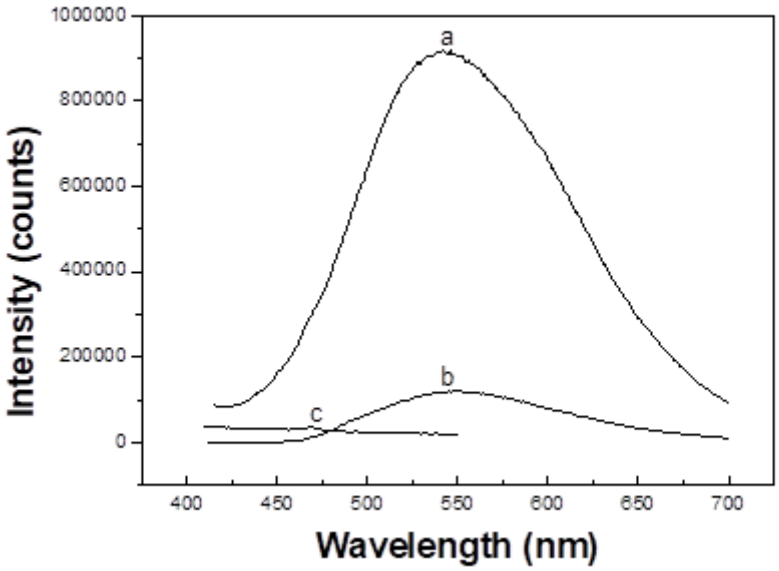

Figure 9

Fluorescence emission spectrum of (a) PI/mSiO2@CdS@CDs, (b) PI/diatomite@CdS@CDs, (c) pure PI

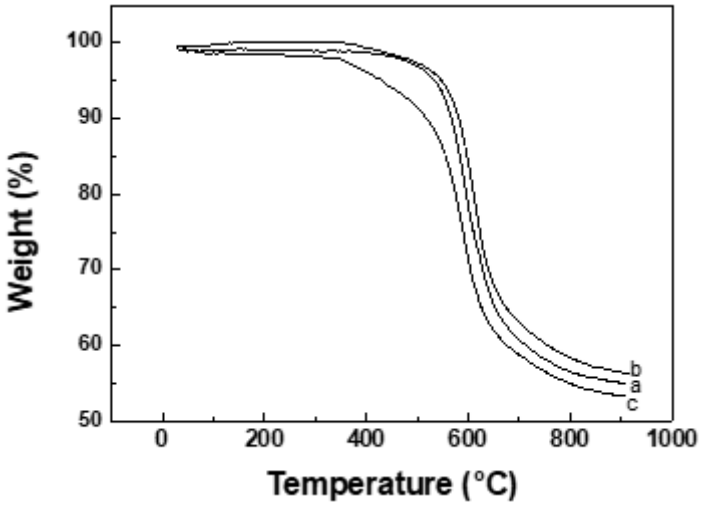

Figure 10

TGA curves of (a) Pure PI, (b) PI/mSiO2@CdS@CDs, (c) PI/diatomite@CdS@CDs

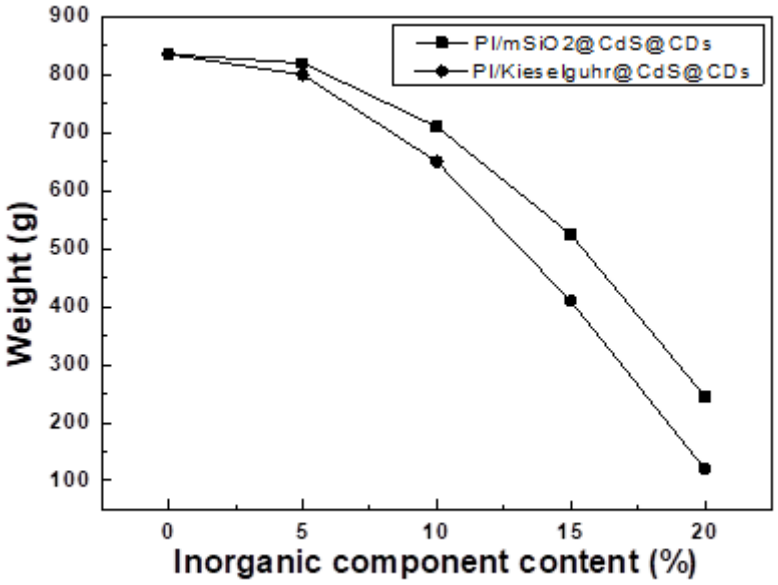

Figure 11

Breaking strength of (a) PI/mSiO2@CdS@CDs, (b) PI/diatomite@CdS@CDs with different inorganic contents